Excited-State Double Exchange in Manganese-Doped ZnO Quantum Dots: A Time-Dependent Density-Functional Study

THE JOURNAL OF PHYSICAL CHEMISTRY Letters

pubs.acs.org/JPCL

Excited-State Double Exchange in Manganese-Doped ZnO Quantum Dots: A Time-Dependent Density-Functional Study

Yong Feng, Ekaterina Badaeva, Daniel R. Gamelin,* and Xiaosong Li*

Department of Chemistry, University of Washington, Seattle, Washington 98195

ABSTRACT The lowest-energy electronic excited states of ZnO quantum dots containing 1−3 Mn^{2+} ions have been studied by time-dependent density functional theory. The calculations show that these excited states involve holes with predominantly manganese 3d character and electrons delocalized in conduction-band-like orbitals, consistent with description of these lowest-energy excited states as charge-transfer (photoionization) states. When the quantum dot contains two or more distant Mn^{2+} ions, spin-dependent hole delocalization among the dopants is observed, with parallel Mn^{2+} spin alignment maximizing hole delocalization and excited state energy stabilization. This effect is proposed to arise from double exchange in the charge-transfer excited state.

SECTION Nanoparticles and Nanostructures

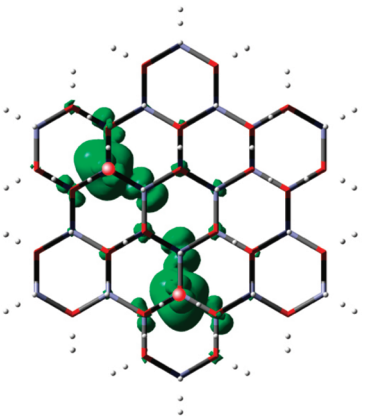

The generation and manipulation of spins in diluted magnetic semiconductor (DMS) nanostructures have been the subject of intense experimental and theoretical investigation owing to potential applications of such materials in spin-based information processing technologies.[1,2] Carrier−dopant magnetic exchange interactions, which underlie such distinctive DMS properties as giant Zeeman and Faraday rotation effects, are being exploited to manipulate either carrier spin polarizations or the spins of magnetic dopants themselves in such nanostructures.[3−5] The recent observation of large, reversible, room-temperature magnetic responses to the introduction and removal of conduction band (CB) electrons in colloidal Mn^{2+}-doped ZnO quantum dots ($Zn_{1-x}Mn_xO$ QDs), despite relatively weak s−d exchange energies, is encouraging in this regard.[6] In principle, introducing a valence band (VB) hole into similar $Zn_{1-x}Mn_xO$ QDs should lead to even greater effects at higher temperatures, but the formation of hole-doped ZnO of any type remains a formidable challenge.

One facile approach to hole generation in semiconductor nanocrystals is charge-carrier photoexcitation. In this work, we theoretically analyze the spin properties of the lowest-energy electronic excited states of $Zn_{1-x}Mn_xO$ QDs formed by charge-carrier photoexcitation. From experiment,[7,8] a defining feature of $Zn_{1-x}Mn_xO$ electronic structure is the presence of a $Mn^{2+/3+}$ ionization level within the ZnO gap. The findings here suggest that this electronic structure can result in a new type of excited-state magnetic polaron that is formed via double exchange. This phenomenon is related to proposed hole-induced magnetic polarons in p-type ZnO, but has the important distinction that problematic static hole doping is circumvented by use of charge-carrier photoexcitation. Whereas excitonic magnetic polarons arising from sp−d exchange have been studied extensively in narrower-gap II−VI DMSs,[5,9,10] to our knowledge photomagnetization in ZnO DMSs has not been explored either experimentally or theoretically.

The excited-state energies, oscillator strengths, and wave functions of ZnO nanocrystals doped with single Mn^{2+} or Co^{2+} ions have been discussed previously and have shown excellent agreement with experimental results.[11] These calculations predict occupied Mn^{2+} 3d orbitals just above the VB edge (Figure 1). A photoexcitation process corresponding formally to the transfer of one of these d electrons into the ZnO CB to form Mn^{3+} (eq 1a) can be achieved at energies lower than band-to-band excitation (eq 1b). As a result, Mn^{2+} dopants introduce new sub-bandgap donor-type charge-transfer (CT, or "photoionization") excited states, referred to here as $ML_{CB}CT$ states.[7,8]

$$Mn^{2+} \xrightarrow{h\nu} Mn^{3+} + e^-_{CB} \qquad (ML_{CB}CT) \qquad (1a)$$

$$Mn^{2+} \xrightarrow{h\nu} Mn^{2+} + e^-_{CB} + h^+_{VB} \qquad (\text{band-to-band}) \qquad (1b)$$

These $ML_{CB}CT$ states in $Zn_{1-x}Mn_xO$ have been studied experimentally using absorption, magnetic circular dichroism, and photocurrent action spectroscopies,[7,8] from which substantial configuration interaction between $ML_{CB}CT$ and band-to-band excited states was concluded. The energies of these CT states have also been proposed to relate to ferromagnetism in bulk $Zn_{1-x}Mn_xO$.[8] For 1.8 nm diameter ZnO QDs with a single Mn^{2+} dopant, the lowest-energy transition is calculated to occur 3.356 eV above the ground state, approximately 1 eV

Received Date: March 26, 2010
Accepted Date: May 31, 2010
Published on Web Date: June 08, 2010

DOI: 10.1021/jz100402q | *J. Phys. Chem. Lett.* **2010**, *1*, 1927–1931

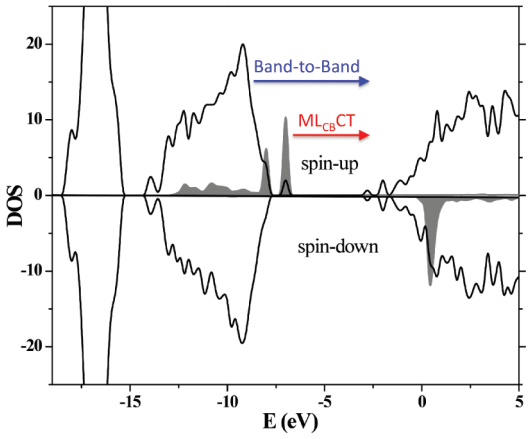

Figure 1. Density of states (DOS) of Mn^{2+}-doped ZnO nanocrystals (84 cations, diameter = 1.8 nm). Shaded regions indicate the partial contributions of Mn^{2+} 3d levels (10-fold magnification). Spin-up and spin-down densities are plotted as positive and negative values, respectively.

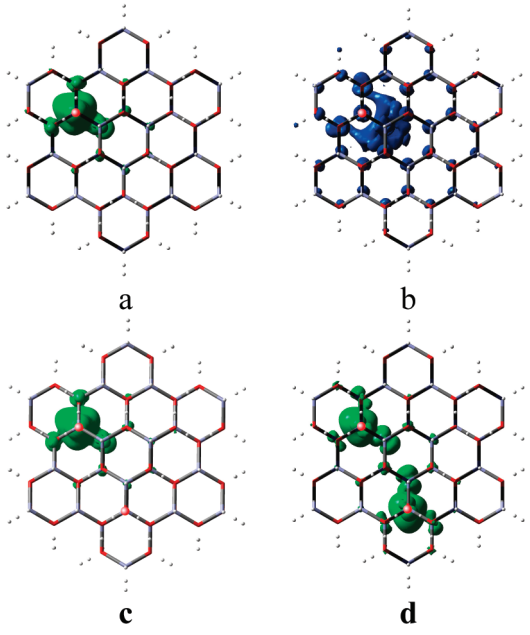

Figure 2. Density distributions for photogenerated carriers in the first electronic excited states of $Zn_{84-N}Mn_NO_{84}$ nanocrystals (diameter = 1.8 nm) with N = 1 or 2, obtained using eq 6. (a) Hole probability density in a $Zn_{83}MnO_{84}$ nanocrystal. (b) Electron probability density in the same nanocrystal. (c) Hole density in a $Zn_{82}Mn_2O_{84}$ nanocrystal with S_{Mn} = 0 (antiferromagnetic), and (d) in the same nanocrystal with S_{Mn} = 5 (ferromagnetic). Red dots indicate the relative positions of Mn^{2+} ions.

below the first band-to-band transition. Figure 2a,b shows probability densities for the photogenerated electron and hole of the lowest-energy excited state, respectively. As anticipated from Figure 1 and eq 1a, the photogenerated hole is localized around the Mn^{2+}, making it Mn^{3+}-like (Figure 2a), and the photogenerated electron has CB-like wave function character and a node at the dopant (Figure 2b).

We now examine the analogous $ML_{CB}CT$ excited states of ZnO QDs containing multiple Mn^{2+} ions using the linear

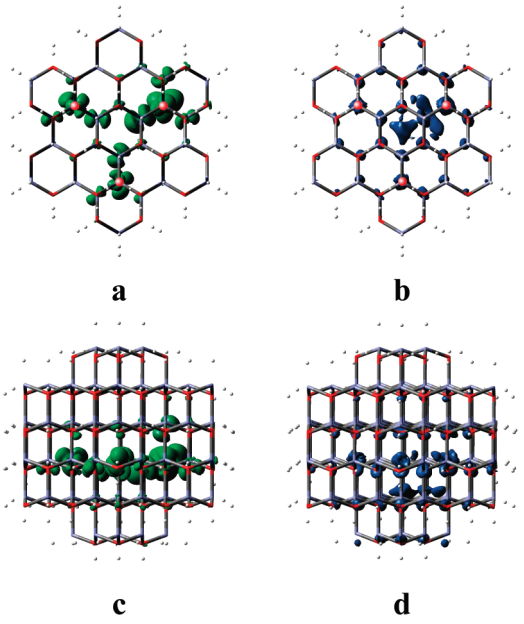

Figure 3. Top- and side-view density distributions for photogenerated holes (a,c) and electrons (b,d) in the lowest excited state of a $Zn_{81}Mn_3O_{84}$ nanocrystal with S_{Mn} = 15/2 (ferromagnetically coupled), obtained using eq 6. Red dots indicate the relative positions of Mn^{2+} ions.

response time-dependent density functional theory (TDDFT) with the PBE1PBE kernel. For these calculations, the additional dopants were positioned at the second nearest-neighbor sites to avoid superexchange coupling, which drops to a negligibly small value at this distance.[6,12] When the spins of the two distant Mn^{2+} ions are antiparallel (S_{Mn} = 0), the $ML_{CB}CT$ energies and the electron and hole wave functions are all similar to those shown in Figure 2a,b, with the hole localized primarily around just one Mn^{2+} ion (Figure 2c). In contrast, the lowest $ML_{CB}CT$ transition shifts ~58 meV to lower energy (to 3.298 eV) when the spins of the two distant Mn^{2+} ions are aligned (S_{Mn} = 5). This energy shift is accompanied by delocalization of the hole over both dopants (Figure 2d), despite their negligible interaction in the ground state. In ZnO QDs with three Mn^{2+} dopants, the lowest electronic excited state is again the $ML_{CB}CT$ state with the highest net spin (S_{Mn} = 15/2), with a photogenerated hole (Figure 3a,c) that is delocalized over all three dopants. The photoexcited electron (Figure 3b,d) is delocalized in the ZnO CB. This high-spin CT state is again stabilized by ~51 meV relative to the $ML_{CB}CT$ energy of the isolated Mn^{2+}, and is now doubly degenerate. The lowest-energy excited states of $Zn_{1-x}Mn_xO$ QDs containing multiple Mn^{2+} ions are thus high-spin $ML_{CB}CT$ states that involve hole delocalization among dopants. This phenomenon was also observed in calculations using short-range screened HSE1PBE and long-range corrected LC-wPBE functionals (stabilization energies: 55 and 70 meV, respectively), indicating that it does not arise from spurious delocalization due to the approximate nature of the DFT kernel.

The above observations bear all the hallmarks of double exchange,[13,14] a phenomenon common among manganites[15,16]

DOI: 10.1021/jz100402q | J. Phys. Chem. Lett. 2010, 1, 1927–1931

and related concentrated magnetic oxides but less commonly considered for diluted magnetic oxides.[17] Before exploring this possibility, we first note that the photogenerated CB electron gives rise to relatively weak s−d exchange coupling, with an average $J_{sd} \sim 0.01$ meV estimated from quantum mechanical calculations[6] and magneto-transport measurements.[18] The effect of the CB electron in the $ML_{CB}CT$ spectrum is thus small compared to the effect of the hole and can be neglected.

To test the hypothesis that the spin-dependent hole delocalization in the $ML_{CB}CT$ excited states of these $Zn_{1-x}Mn_xO$ QDs results from double exchange, the properties anticipated from true double exchange were explored using the Anderson−Hasegawa (AH) model,[14] which neglects important local effects such as electron−nuclear coupling or zero-field splittings but nevertheless captures the essence of the phenomenon. In the AH model, the interaction Hamiltonian for two distant Mn^{2+} ions coupled by an itinerant photogenerated hole can be written as in eq 2:

$$H = \begin{array}{c} \\ \mathrm{Mn}_i^{2+}:h^+ \\ \mathrm{Mn}_j^{2+}:h^+ \end{array} \begin{array}{c} \begin{array}{cc} \mathrm{Mn}_i^{2+}:h^+ & \mathrm{Mn}_j^{2+}:h^+ \end{array} \\ \begin{pmatrix} 0 & t_{ij}\dfrac{(S_T-1/2)}{2S-1} \\ t_{ij}\dfrac{(S_T-1/2)}{2S-1} & 0 \end{pmatrix} \end{array} \quad (2)$$

where t_{ij} is the absolute-value intermanganese transfer integral, and S_T (9/2, 7/2, ... 1/2) and S (5/2) are the total spin ($2Mn^{2+} + h^+$) and localized spin (Mn^{2+}), respectively. The diagonal elements of eq 2 are set to zero to reflect the negligible superexchange coupling between anything but nearest-neighbor Mn^{2+} ions in the ZnO lattice.[6,12] The $ML_{CB}CT$ transition energy of a QD with only one Mn^{2+} dopant thus serves as the reference energy ($E = 0$).

Diagonalizing eq 2 yields a non-Heisenberg spin ladder with energies of $E_{S_T} = \pm t_{ij}\frac{(S_T-1/2)}{2S-1}$, in which the state with the highest total spin ($S_T = 9/2$) is stabilized by energy t_{ij} upon hole delocalization. The state with the lowest total spin ($S_T = 1/2$) does not gain any stabilization from hole delocalization and thus has energy $E_{1/2} = 0$.

Equation 2 is readily extended to N ions (eq 3). Diagonalizing eq 3 yields N possible high-spin states, including $N - 1$ degenerate lowest-energy levels at $E_- = -t_{ij}[(S_T - 1/2)/(2S - 1)]$, and one high-energy level at $E_+ = t_{ij}(N - 1)[(S_T - 1/2)/(2S - 1)]$.

$$H = \begin{array}{c} \\ \mathrm{Mn}_i^{2+}:h^+ \\ \mathrm{Mn}_j^{2+}:h^+ \\ \mathrm{Mn}_k^{2+}:h^+ \\ \vdots \end{array} \begin{array}{c} \begin{array}{ccc} \mathrm{Mn}_i^{2+}:h^+ & \mathrm{Mn}_j^{2+}:h^+ & \mathrm{Mn}_k^{2+}:h^+ \quad \cdots \end{array} \\ \begin{pmatrix} 0 & t_{ij}\dfrac{(S_T-1/2)}{2S-1} & t_{ik}\dfrac{(S_T-1/2)}{2S-1} \quad \cdots \\ t_{ij}\dfrac{(S_T-1/2)}{2S-1} & 0 & t_{jk}\dfrac{(S_T-1/2)}{2S-1} \quad \cdots \\ t_{ik}\dfrac{(S_T-1/2)}{2S-1} & t_{jk}\dfrac{(S_T-1/2)}{2S-1} & 0 \quad \cdots \\ \vdots & \vdots & \vdots \quad \ddots \end{pmatrix} \end{array} \quad (3)$$

These equations now allow the computational results described above to be understood. For ZnO QDs with two dopants, eq 2 predicts that double exchange will stabilize one high-spin $ML_{CB}CT$ state by an energy t_{ij}, and for QDs with three dopants eq 3 predicts stabilization of two high-spin $ML_{CB}CT$ states by t_{ij} each. Note that the positive sign of t_{ij} follows from the symmetry of the oxo p orbitals mediating the exchange, as this requires a phase change between participating Mn^{2+} 3d orbitals. The AH model thus precisely anticipates the results of the DFT calculations, strongly supporting the conclusion that double exchange is responsible for the spin-dependent hole delocalization found in the DFT results. Furthermore, from eq 2 the $ML_{CB}CT$ energy stabilization upon hole delocalization onto a second Mn^{2+} directly yields the double-exchange coupling energy, i.e., $t_{ij} \approx 58$ meV for the nanocrystal of Figure 2d. Although smaller than those in manganites[15,16] or some molecular systems,[19] this value exceeds kT at room temperature.

This excited-state double exchange was explored more generally by considering different locations of the Mn^{2+} ions within these diameter = 1.8 nm QDs, and by considering QDs of different dimensions. The value of t_{ij} was found to depend on the positions of the Mn^{2+} ions within the QDs, growing weaker as the dopants were moved toward the QD edges and as the distance between dopants was increased. For example, increasing the dopant separation from second to third nearest neighbor reduces t_{ij} from 58 to less than 10 meV in the 1.8 nm QDs. Similarly, keeping the dopants fixed but removing one ZnO monolayer (i.e., reducing the cluster size from 84 to 33 cations) reduces t_{ij} from 58 to 50 meV. These observations are interpreted as reflecting participation of the ZnO VB in the double exchange pathway. Because the dopants do not directly neighbor one another, a nonzero interdopant hole-transfer integral is only possible if the hole wave function possesses an admixture of delocalized VB character in its otherwise localized 3d parent function. From second-order perturbation theory, the intermanganese transfer integral (t_{ij}) depends on the squared dopant-VB transfer integral, ($t_{d\text{-}VB}$, which is itself proportional to the dopant-VB overlap integral) and the energy difference between the relevant 3d orbitals and the VB edge ($\Delta E_{d\text{-}VB}$), as described by eq 4.[14] Because the Mn^{2+} 3d orbitals reside only slightly above the ZnO VB edge (Figure 1), $\Delta E_{d\text{-}VB}$ is small and the photogenerated hole is energetically well positioned to take on substantial VB wave function character. Similarly, because the VB envelope function tends toward zero at the QD surfaces, displacement of Mn^{2+} toward the surface diminishes t_{ij}.

$$t_{ij} \sim \frac{(t_{d-VB})^2}{\Delta E_{d-VB}} \quad (4)$$

Quantification of the result in Figure 2a indicates that ~30% of the hole probability density lies beyond the first coordination sphere of the dopant, reflecting partial hole delocalization into the VB through configuration interaction. This partial delocalization can be described as a finite hole effective radius, r_B, derived from the small Mn^{2+}-h^+ binding energy, E_b (eq 5).

$$r_B = \frac{\hbar}{\sqrt{2m^*E_b}} \quad (5)$$

From experiment, $r_B \sim 0.45$ nm has been estimated for the Mn^{2+}-h^+ complex in $Zn_{1-x}Mn_xO$,[8] which compares well with the value of ~0.45−0.50 nm estimated here from the DFT wave functions. In contrast with the particle-in-a-box model of eq 5, the DFT results illustrate how this hole

DOI: 10.1021/jz100402q | J. Phys. Chem. Lett. 2010, 1, 1927–1931

probability distribution is not spherical but atomistic. Overall, we conclude that the phenomenon of excited-state double exchange in $Zn_{1-x}Mn_xO$ QDs is made possible by the substantial (greater than ~30%) VB character of the photogenerated hole's wave function, despite its predominantly manganese 3d character. A remaining open question pertains to the extent of hole localization that might arise from electron−nuclear coupling, which has been neglected in the calculations presented here. We note that reduced confinement will bring the first interband excited state closer in energy to the lowest CT level,[11] which will reduce the hole binding energy and lessen the electron−nuclear coupling energy. Calculations to address this consideration are presently underway.

The excited-state double exchange phenomenon described here has not been discussed previously. It differs fundamentally from the excitonic magnetic polaron phenomenon known in other II−VI DMSs because it occurs in the $ML_{CB}CT$ state, but it can be related to proposals of bound magnetic polarons (BMPs), impurity bands, and ferromagnetism in bulk $Zn_{1-x}Mn_xO$ and some bulk manganese-doped III−V DMSs. A double-exchange model of ferromagnetism in Mn-doped III−V semiconductors has been proposed.[20] In bulk p-$Zn_{1-x}Mn_xO$, manganese-based hole delocalization to form a magnetic impurity band was proposed.[8,17,21] The present study describes double-exchange ferromagnetic coupling initiated by QD photoexcitation, but very similar computational results are also obtained when the electron is removed entirely. The excited-state double exchange described here is thus directly analogous to the proposed BMP formation of bulk p-type $Zn_{1-x}Mn_xO$. Given the typical DMS spin ordering times of only a few hundred picoseconds under p−d exchange fields,[5,9,10] even relatively short-lived excited states may allow photomagnetization by this mechanism. Charge separation by electric fields or type II heterostructures could be exploited to elongate hole lifetimes generated by CT excitation, enhancing the effect.

THEORETICAL METHODS

The electronic excited state energies of $Zn_{1-x}Mn_xO$ QDs were calculated using TDDFT within the linear response framework. All calculations were performed with the development version of the Gaussian program suite.[22] Nanocrystal electronic structures were obtained with the PBE1PBE hybrid DFT functional.[23−25] Short-range screened hybrid HSE1-PBE[26−28] functional and long-range corrected LC-wPBE[29,30] functional were also used to check for possible spurious delocalization. The TDDFT kernel used in this work is within the adiabatic approximation, in which the ground state exchange-correlation kernel is used for excited state calculations. Our previous work[11] using the adiabatic approximation of the exchange-correlation kernel in linear response TDDFT has yielded CT and band-to-band transition energies and intensities in $Zn_{1-x}Mn_xO$ QDs that agree well with experiment, suggesting that the calculations also describe the wave functions well. The Los Alamos double-ζ pseudocore potential (LANL2DZ)[31−34] and the associated basis set were used for all atoms, with the Zn (4s, 3d), Mn (3s, 3p, 4s, 3d), and O (1s, 2s, 2p) electrons treated as valence electrons. Wurtzite ZnO ($Zn_{84}O_{84}$) nanocrystals with C_{3v} symmetry were constructed according to the scheme described in ref 35. Lattice parameters were obtained from experiment: a = 3.249 Å, c = 5.204 Å, and u = 0.382.[36] Dangling bonds on the nanocrystal surfaces were passivated with pseudohydrogen atoms, which have modified nuclear charges of 0.5 and 1.5 to terminate surface O^{2-} and Zn^{2+} ions, respectively. The O−H and Zn−H bonds were fully optimized. This pseudohydrogen capping scheme leads to a well-defined bandgap and a stable nanocrystal geometry (see ref 35 for details). When Mn^{2+} is doped into the ZnO nanocrystal, it substitutes for a Zn^{2+} ion keeping the total charge of the cluster neutral. Using this computational approach, properties of both ground and excited states can be addressed, and additional positive or negative charge carriers can also be introduced with full wave function optimization.[6] To describe the electronic excited states, changes in electron- and hole-density distributions that result from photoexcitation were analyzed. The photogenerated electron ($\rho_e(r)$) and hole ($\rho_h(r)$) distributions are defined as the positive and negative electron density differences between the excited and ground states (eq 6),

$$\rho_e(r) = [\rho_n(r) - \rho_0(r)]^+ \quad (6a)$$

$$\rho_h(r) = [\rho_n(r) - \rho_0(r)]^- \quad (6b)$$

where $\rho_n(r)$ and $\rho_0(r)$ are total electron density distributions of the fully optimized and self-consistent excited and ground state wave functions, respectively, neglecting relaxation of nuclear coordinates.

AUTHOR INFORMATION

Corresponding Author:

*To whom correspondence should be addressed. E-mail: li@chem.washington.edu; tel: 206-685-1804; fax: 206-685-8665 (X.L.). E-mail: gamelin@chem.washington.edu; tel: 206-685-0901; fax: 206-685-8665 (D.R.G.).

ACKNOWLEDGMENT This work was supported by the U.S. National Science Foundation (CHE 0628252-CRC to D.R.G. and X.L.). E.B. thanks the UW Center for Nanotechnology for a UIF fellowship. Additional support from Gaussian Inc., the Research Corporation, the Dreyfus Foundation, and the University of Washington Student Technology Fund is gratefully acknowledged.

REFERENCES

(1) Zutic, I.; Fabian, J.; Das Sarma, S. Spintronics: Fundamentals and Applications. *Rev. Mod. Phys.* **2004,** *76*, 323–410.
(2) Wolf, S. A.; Awschalom, D. D.; Buhrman, R. A.; Daughton, J. M.; von Molnár, S.; Roukes, M. L.; Chthelkanova, A. Y.; Treger, D. M. Spintronics: A Spin-Based Electronics Vision for the Future. *Science* **2001,** *294*, 1488–1495.
(3) Ohno, Y.; Young, D. K.; Beschoten, B.; Matsukura, F.; Ohno, H.; Awschalom, D. D. Electrical Spin Injection in a Ferromagnetic Semiconductor Heterostructure. *Nature* **1999,** *402*, 790–792.
(4) Jonker, B. T.; Park, Y. D.; Bennett, B. R.; Cheong, H. D.; Kioseoglou, G.; Petrou, A. Robust Electrical Spin Injection into a Semiconductor Heterostructure. *Phys. Rev. B* **2000,** *62*, 8180–8183.

DOI: 10.1021/jz100402q | *J. Phys. Chem. Lett.* **2010,** *1*, 1927–1931

(5) Beaulac, R.; Schneider, L.; Archer, P. I.; Bacher, G.; Gamelin, D. R. Light-Induced Spontaneous Magnetization in Colloidal Doped Quantum Dots. *Science* **2009,** *325*, 973–976.
(6) Ochsenbein, S. T.; Feng, Y.; Whitaker, K. M.; Badaeva, E.; Liu, W. K.; Li, X.; Gamelin, D. R. Charge-Controlled Magnetism in Colloidal Doped Semiconductor Nanocrystals. *Nat. Nanotechnol.* **2009,** *4*, 681–687.
(7) Norberg, N. S.; Kittilstved, K. R.; Amonette, J. E.; Kukkadapu, R. K.; Schwartz, D. A.; Gamelin, D. R. Synthesis of Colloidal Mn^{2+}:ZnO Quantum Dots and High-T_c Ferromagnetic Nanocrystalline Thin Films. *J. Am. Chem. Soc.* **2004,** *126*, 9387–9398.
(8) Kittilstved, K. R.; Liu, W. K.; Gamelin, D. R. Electronic Structure Origins of Polarity Dependent High-T_c Ferromagnetism in Oxide Diluted Magnetic Semiconductors. *Nat. Mater.* **2006,** *5*, 291–297.
(9) Harris, J. H.; Nurmikko, A. V. Formation of the Bound Magnetic Polaron in (Cd,Mn)Se. *Phys. Rev. Lett.* **1983,** *51*, 1472–1475.
(10) Seufert, J.; Bacher, G.; Scheibner, M.; Forchel, A.; Lee, S.; Dobrowolska, M.; Furdyna, J. K. Dynamical Spin Response in Semimagnetic Quantum Dots. *Phys. Rev. Lett.* **2002,** *88*, 027402.
(11) Badaeva, E.; Isborn, C. M.; Feng, Y.; Ochsenbein, S. T.; Gamelin, D. R.; Li, X. Theoretical Characterization of Electronic Transitions in Co^{2+}- and Mn^{2+}-Doped ZnO Nanocrystals. *J. Phys. Chem. C* **2009,** *113*, 8710–8717.
(12) Kolesnik; Dabrowski; Wiren; Kepa; Giebultowicz; Brown; Lëao; Furdyna, J. K. Determination of Antiferromagnetic Interactions in Zn(Mn)O, Zn(Co)O, and Zn(Mn)Te by Inelastic Neutron Scattering. *J. Appl. Phys.* **2006,** *99*, 08M122.
(13) Zener, C. Interaction between the D-Shells in the Transition Metals. II. Ferromagnetic Compounds of Manganese with Perovskite Structure. *Phys. Rev.* **1951,** *82*, 403–405.
(14) Anderson, P. W.; Hasegawa, H. Considerations on Double Exchange. *Phys. Rev.* **1955,** *100*, 675–681.
(15) Coey, J. M. D.; Viret, M.; von Molnár, S. Mixed-Valence Manganites. *Adv. Phys.* **1999,** *48*, 167–293.
(16) Edwards, D. M. Ferromagnetism and Electron-Phonon Coupling in the Manganites. *Adv. Phys.* **2002,** *51*, 1259–1318.
(17) Sato, K.; Katayama-Yoshida, H. Ferromagnetism in a Transition Metal Atom Doped ZnO. *Physica E* **2001,** *10*, 251–255.
(18) Andrearczyk, T.; Jaroszyñski, J.; Grabecki, G.; Dietl, T.; Fukumura, T.; Kawasaki, M. Spin-Related Magnetoresistance of *N*-Type ZnO:Al and $Zn_{1-x}Mn_xO$:Al Thin Films. *Phys. Rev. B* **2005,** *72*, 121309.
(19) Gamelin, D. R.; Bominaar, E. L.; Kirk, M. L.; Wieghardt, K.; Solomon, E. I. Excited-State Contributions to Ground-State Properties of Mixed-Valence Dimers: Spectral and Electronic-Structural Studies of $[Fe_2(OH)_3(tmtacn)_2]^{2+}$ Related to the $[Fe_2S_2]^{+}$ Active Sites of Plant-Type Ferredoxin. *J. Am. Chem. Soc.* **1996,** *118*, 8085–8097.
(20) Krstajić, P. M.; Peeters, F. M.; Ivanov, V. A.; Fleurov, V.; Kikoin, K. Double-Exchange Mechanisms for Mn-Doped III−V Ferromagnetic Semiconductors. *Phys. Rev. B* **2004,** *70*, 195215.
(21) Wang, Q.; Sun, Q.; Jena, P.; Kawazoe, Y. Carrier-Mediated Ferromagnetism in N Codoped (Zn,Mn)O $(10\bar{1}0)$ Thin Films. *Phys. Rev. B* **2004,** *70*, 052408.
(22) Frisch, M. J.; Trucks, G. W.; Schlegel, H. B.; Scuseria, G. E.; Robb, M. A.; Cheeseman, J. R.; Montgomery, J. A.; Vreven., T.; Scalmani, G.; Mennucci, B.; et al. *Gaussian Development Version*, revision H01; Gaussian, Inc.: Wallingford, CT, 2009.
(23) Perdew, J. P.; Burke, K.; Ernzerhof, M. Generalized Gradient Approximation Made Simple. *Phys. Rev. Lett.* **1996,** *77*, 3865–3868.
(24) Perdew, J. P.; Burke, K.; Ernzerhof, M. Generalized Gradient Approximation Made Simple [Erratum]. *Phys. Rev. Lett.* **1997,** *78*, 1396.
(25) Adamo, C.; Barone, V. Toward Reliable Density Functional Methods without Adjustable Parameters: The PBE0Model. *J. Chem. Phys.* **1999,** *110*, 6158–6170.
(26) Heyd, J.; Scuseria, G. E. Assessment and Validation of a Screened Coulomb Hybrid Density Functional. *J. Chem. Phys.* **2004,** *120*, 7274–7280.
(27) Heyd, J.; Scuseria, G. E. Efficient Hybrid Density Functional Calculations in Solids: Assessment of the Heyd−Scuseria−Ernzerhof Screened Coulomb Hybrid Functional. *J. Chem. Phys.* **2004,** *121*, 1187–1192.
(28) Heyd, J.; Scuseria, G. E.; Ernzerhof, M. Hybrid Functionals Based on a Screened Coulomb Potential. *J. Chem. Phys.* **2003,** *118*, 8207–8215.
(29) Vydrov, O. A.; Heyd, J.; Krukau, A. V.; Scuseria, G. E. Importance of Short-Range Versus Long-Range Hartree−Fock Exchange for the Performance of Hybrid Density Functionals. *J. Chem. Phys.* **2006,** *125*, 074106.
(30) Vydrov, O. A.; Scuseria, G. E. Assessment of a Long-Range Corrected Hybrid Functional. *J. Chem. Phys.* **2006,** *125*, 234109.
(31) Dunning, T. H.; Hay, P. J. In *Modern Theoretical Chemistry*; Shaefer, H. F., Ed.; Plenum: New York, 1977; Vol. 3; pp 1.
(32) Hay, P. J.; Wadt, W. R. Ab Initio Effective Core Potentials for Molecular Calculations. Potentials for the Transition Metal Atoms Sc to Hg. *J. Chem. Phys.* **1985,** *82*, 270–283.
(33) Wadt, W. R.; Hay, P. J. Ab Initio Effective Core Potentials for Molecular Calculations. Potentials for Main Group Elements Na to Bi. *J. Chem. Phys.* **1985,** *82*, 284–298.
(34) Hay, P. J.; Wadt, W. R. Ab Initio Effective Core Potentials for Molecular Calculations. Potentials for K to Au Including the Outermost Core Orbitals. *J. Chem. Phys.* **1985,** *82*, 299–310.
(35) Badaeva, E.; Feng, Y.; Gamelin, D. R.; Li, X. Investigation of Pure and Co^{2+}-Doped ZnO Quantum Dot Electronic Structures Using Density Functional Theory: Choosing the Right Functional. *New J. Phys.* **2008,** *10*, 055013.
(36) Kisi, E. H.; Elcombe, M. M. *U* Parameters for the Wurtzite Structure of ZnS and ZnO Using Powder Neutron Diffraction. *Acta Crystallogr.* **1989,** *C45*, 1867–1870.

DOI: 10.1021/jz100402q | *J. Phys. Chem. Lett.* **2010,** *1*, 1927–1931